Bayesian estimation of human impedance and motion intention for human-robot collaboration

Article (Accepted Version)

Bayesian Estimation of Human Impedance and Motion Intention for Human-Robot Collaboration

Xinbo Yu, *Student Member, IEEE,* Wei He, *Senior Member, IEEE,* Yanan Li, *Member, IEEE*, Chengqian Xue, Jianqiang Li, Jianxiao Zou, *Member, IEEE* and Chenguang Yang, *Senior Member, IEEE*

***Abstract*—This paper proposes a Bayesian method to acquire the estimation of human impedance and motion intention in a human-robot collaborative task. Combining with prior knowledge of human stiffness, estimated stiffness obeying Gaussian distribution is obtained by Bayesian estimation and human motion intention can be also estimated. An adaptive impedance control strategy is employed to track a target impedance model and neural networks are used to compensate for uncertainties in robotic dynamics. Comparative simulation results are carried out to verify the effectiveness of estimation method and emphasize the advantages of the proposed control strategy. The experiment, performed on Baxter® robot platform, illustrate a good system performance.**

***Index Terms*—neural networks, adaptive impedance control, human impedance, human motion intention estimation, Bayesian estimation.**

I. Introduction

Service robots are becoming more significant in our daily lives and help human partners at home or in social environments [1]–[4]. Considering many tasks that need at least two persons to complete, such as moving a table, one person finds difficulties due to limits of the maximum extension of human arm and human load ability, so it needs another person ("co-operator") to cooperate with him/her ("initiator"). To ensure finishing the task successfully, the "initiator" should perceive a precise ordered location and know prior task processes, but more than that, the movement of this "cooperator" should be compliant to the motion of "initiator" completely. It means that "cooperator" will need to know motion intention of "initiator" and adapt to movement and interaction force of "initiator". Obviously, collaborative robots, which are centered on human task requirement, have the ability to assist human partner and supersede "cooperator" work in such kind of tasks [5]–[8].

This work was supported in part by the National Natural Science Foundation of China under Grant 61933001, Grant 61873298, Grant 61622308, Grant 61873206, in part by the Natural Science Foundation of Beijing Municipality under Grant 4172041, and in part by the Joint Fund of Equipment Pre-Research and Ministry of Education under Grant 6141A02033339.

X. Yu, W. He and C. Xue are with the School of Automation and Electrical Engineering, Institute of Artificial Intelligence, University of Science and Technology Beijing, Beijing 100083, China. The corresponding author is W. He, Email: weihe@ieee.org.

Y. Li is with the Department of Engineering and Design, University of Sussex, Brighton, BN1 9RH, UK.

J. Li is with the College of Computer Science and Software Engineering, Shenzhen University, Shenzhen 518060, China.

J. Zou is with the School of Automation Engineering, University of Electronic Science and Technology of China, Chengdu 611731, China.

C. Yang is with the College of Automation Science and Engineering, South China University of Technology, Guangzhou 510641, China.

Let us consider a classical physical human-robot interaction (pHRI) scenario as in Fig. 1. Abundant control strategies are developed for pHRI [9], [10] and various adaptive or learning control strategies also draw much attention from scholars [11]–[16]. Impedance control, firstly proposed by Hogan [17], is used to relate interactive force with deviations from desired states. Adaptive impedance control methods are proposed subsequently, e.g., [18]–[21]. Compared with hybrid force/position control, impedance control shows better robustness and does not need transitions between contact and non-contact situations. Although traditional impedance control has shown good performance in pHRI [22], it only enables human to change the robot's actual trajectory but not the robot's desired trajectory [23]. If robot has knowledge of human motion intention [24], it can regard human motion intention as its own desired trajectory and human will cost less effort to accomplish the task. In [25], human motion intention has been estimated by online neural networks (NNs) based on available sensory information, an updating law is designed and the robot moves to time-varying human's intended position actively. In [26], an inversion-based approach is proposed to estimate the human intent by demonstration and it is used in input updating for improving trajectory tracking accuracy. The effectiveness of human guided iterative learning control has been proven by human-in-loop trajectory tracking experiment. [27] proposes a method to predict the next movement of the human partner who is collaborating with robot by applying inverse optimal control and goal set iterative replanning. In [28], human motion intention is identified to enable the robot to follow human compliantly in fast point-to-point tasks.

When robot interacts with human in a constrained motion form, an estimation method of human impedance should be considered for improving the system stability during pHRI [29]–[32]. By tuning a target impedance based on human impedance estimation, variable target impedance parameters extend the robot learning skills beyond trajectory tracking, in which robot is gifted with submissive performance and more advanced skills that involve, among others, contacting with human partner. Some common contact impedance estimation methods are analyzed in [33], which include recursive least squares method, model reference and indirect adaptive method and signal processing method. Using information extracted from programming by human demonstration, [34] proposes a method to estimate environmental stiffness which is obtained according to covariance of Gaussian mixture model. In [35], the tutor transfers a specific sawing skill to the robot successfully, by using electromyography (EMG) signals to estimate

tutor stiffness in pHRI. In [36], desired impedance parameters are obtained based on gradient-following and betterment methods. In [37], the optimal desired stiffness is designed by using human operator's electromyography (EMG) signals in an upper limb robotic exoskeleton application. In [38], [39], in order to estimate human impedance characteristics, a small external perturbation to the human arm is required in the cooperative task.

Abundant control strageties of nonlinear systems are proposed in recent years [40]–[44]. Model-based control strategies have more precise tracking capacities than classical PID control. In addition it can avoid spending time finding proper PID values of gains. The researches on adaptive control also draw much attention [45]–[47]. However, uncertainties in model dynamics are ubiquitous [48], [49] and have attracted attention of researchers [50]–[54]. In [55], radial basis function neural networks (RBFNN) are used to handle uncertainties in robotic dynamics, and the back-stepping method is used to design a stable controller. This RBFNN method has been used in applications of robotic flexible joints [56], output and input constraints [57]–[62] and teleoperation [63]. In [64], NN are employed to compensate for uncertainties in the presence of unknown dynamics of both the grasped object and dual robotic manipulators. A switching method is integrated into controller to achieve global stability. In [65], an adaptive robust control design is proposed for multiple mobile manipulators, a common object in contact with a rigid surface is grasped by multiple mobile manipulators and they show robustness not only to parametric uncertainties but also to external disturbances. Some observer-based adaptive control strategies are also proposed for solving unknown disturbance or unknown states [66]–[71].

Bayesian estimated methods are widely utilized in dealing with uncertainties in robot motion planning [72] and robot visual tracking [73]. Some works have been done about tactile perception in recent years [74]. In this paper, a Bayesian method is proposed for human impedance and motion intention estimation, and neural impedance control strategy is used to achieve efficient human-robot cooperation.

The construction of this paper is described as follows: in Section II, the dynamics of human and robot are presented and the task objective is introduced; in Section III, a Bayesian estimation method is employed in human stiffness estimation, and the human motion intention is estimated according to the dynamic relationship between human stiffness and motion intention; in Section IV, impedance control is analyzed, NNs are used to handle model uncertainties in control design, and stability analysis is proved by constructing Lyapunov function candidates; in Section V, comparative simulations are carried out to show the advancement of our proposed method; in Section VI, an experiment is designed to evaluate the performance of our controller design on Baxter® robot platform; in Section VII, conclusion is presented.

II. Problem formulation

In this paper, we consider an object transporting task as shown in Fig. 1. In this task, human will lead by applying an interaction force to the object and robot will cooperate with human to lift the object on the other side.

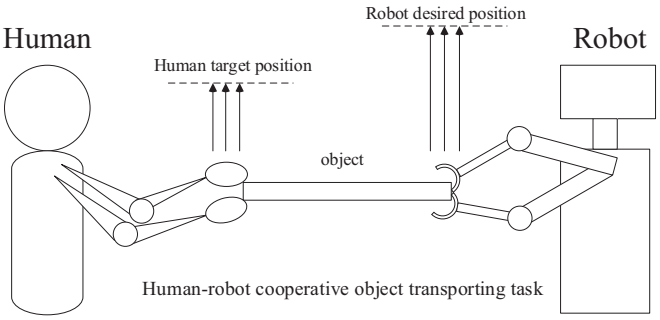

Fig. 1: A scenario where human and robot collaborate to perform an object transporting task. Human is an "initiator" of the task, i.e., human will lead the task and he/she knows the task target position, and robot will be obedient completely to help human to finish the task, i.e., robot will be a "cooperator".

A. Dynamics

I. Robot's Dynamic Model

We consider the robot as an m-DOF rigid manipulator, so the robotic dynamics in joint space can be described as follows

$$M(q)\ddot{q} + C(q,\dot{q})\dot{q} + G(q) = J^T(q)f_r + \tau, \tag{1}$$

where q, $\dot{q}$, $\ddot{q} \in \mathbb{R}^m$ are the joint angle, velocity and acceleration vectors, respectively. $M(q) \in \mathbb{R}^{m\times m}$ is the symmetric and positive definite inertia matrix, $C(q,\dot{q})\dot{q} \in \mathbb{R}^m$ is Coriolis and centripetal vector, $G(q) \in \mathbb{R}^m$ denotes gravity vector, $\tau \in \mathbb{R}^m$ denotes control input vector, $f_r \in \mathbb{R}^h$ is the vector of the interaction force between the robot and the transferred object, $J(q) \in \mathbb{R}^{h\times m}$ is the Jacobian matrix, where h denotes the dimension in Cartesian space. The forward kinematics of the robot is given by $x = \Phi(q)$, differentiating x with respect to time we get $\dot{x} = J(q)\dot{q}$. Based on inverse kinematics, $\dot{q}$ and $\ddot{q}$ in joint space can be described as

$$\begin{aligned} \dot{q} &= J^{-1}(q)\dot{x} \\ \ddot{q} &= \dot{J}^{-1}(q)\dot{x} + J^{-1}(q)\ddot{x}, \end{aligned} \tag{2}$$

where $J^{-1}(q)$ denotes the inverse of $J(q)$, x, $\dot{x}$, $\ddot{x} \in \mathbb{R}^h$ denote the position, velocity and acceleration vectors in Cartesian space, respectively. By substituting (2) into (1), we obtain robot's dynamic model in Cartesian space as follows

$$M_r(x)\ddot{x} + C_r(x,\dot{x})\dot{x} + G_r(x) = u + f_r, \tag{3}$$

where the inertia matrix $M_r(x) \in \mathbb{R}^{h\times h}$, the Coriolis and centripetal force vector $C_r(x,\dot{x})\dot{x} \in \mathbb{R}^h$, the gravitational force vector $G_r(x) \in \mathbb{R}^h$ and the control force vector $u \in \mathbb{R}^h$ in the Cartesian space in (3) can be calculated as

$$\begin{aligned} M_r(x) &= J^{-T}(q)M(q)J^{-1}(q) \\ C_r(x,\dot{x}) &= J^{-T}(q)(C(q,\dot{q}) - M(q)J^{-1}(q)\dot{J}(q))J^{-1}(q) \\ G_r(x) &= J^{-T}(q)G(q) \\ u &= J^{-T}(q)\tau. \end{aligned} \tag{4}$$

II. Human's Dynamic Model

In pHRI, the dynamic model of human in Cartesian space in h dimension can be simply described as a spring model

$$f_h = K_h(x_h - x), \tag{5}$$

where $K_h \in \mathbb{R}^{h\times h}$ denotes human's stiffness matrix, $x_h \in \mathbb{R}^h$ denotes human's target position vector in h dimension, i.e., human motion intention, $x \in \mathbb{R}^h$ denotes actual position, and $f_h \in \mathbb{R}^h$ denotes the interaction force vector between human and transferred object.

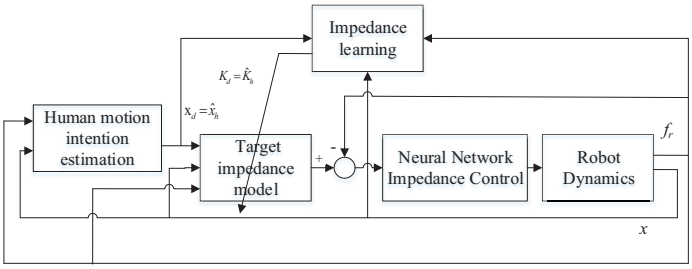

Fig. 2: Control Architecture

B. Task objective

In this task, the most important problems are how to acquire human stiffness and how to obtain human motion intention in (5). If robot knows human motion intention and human stiffness, it will be convenient to design impedance controller for efficient human-robot interaction. In our task, we want to make human and robot act with a same behavior for performing tasks successfully. If they have different behaviors during a cooperative task, the task will be inefficient or unsuccessful. The same behavior means that the robot and human have a same initial position and a same moving target position, and the human's stiffness matrix K_h should be same as the robot's stiffness matrix K_d. Therefore, we firstly design a target impedance model for the robot, which is described as below:

$$-f_r = \Lambda_d(\ddot{x}_d - \ddot{x}) + D_d(\dot{x}_d - \dot{x}) + K_d(x_d - x). \tag{6}$$

where Λ_d is the desired inertia matrix, D_d is the desired damper matrix, K_d is the desired stiffness matrix, and x_d denotes the robot's desired target position. Considering a slow speed human-robot interactive process, (6) can be simplified as

$$-f_r = K_d(x_d - x), \tag{7}$$

because $\dot{x}$ and $\ddot{x}$ are close to zero. The simplified target impedance model (7) shows dynamic relationship between displacement and interaction force clearly. As it can be seen from (5), in this cooperative object transporting task, we should design the robot desired target position x_d as human motion intention x_h and design K_d as human stiffness K_h. However, human motion intention x_h and human stiffness K_h are unknown to robot. Therefore, we need to propose an estimation method to obtain an estimate of human motion intention $\hat{x}_h$ and an estimate of human stiffness $\hat{K}_h$. We can write the estimate of (5) in one dimension as below

$$\hat{f}_{h1} \quad = \quad \hat{K}_{h1}(\hat{x}_{h1} - x_1), \tag{8}$$

where $\hat{K}_{h1}$, $\hat{x}_{h1}$ and $\hat{f}_{h1}$ denote the estimates of human stiffness parameter, human target position and interaction force between human and object in one dimension, respectively.

In this paper, we regard the transporting object as a mass point of which the tiny mass and volume can be ignored. Therefore, the interaction force between human and transferred object f_h is the same as the interaction force between robot and transferred object f_r. This leads to a scenario where human and robot has a direct physical contact. When we measure f_r by the force sensor mounted on the end-effector of robot, f_h can be obtained.

The control architecture is shown in Fig. 2. In the following two sections, we first explain how to estimate human's target position and stiffness, and then design a controller to achieve desired robot's impedance.

III. Human stiffness learning and motion intention estimation

Bayesian parameter estimation method is an important method to estimate unknown parameters. We use this method to get the estimation of K_{h1} and x_{h1}.

First, we establish a quadratic cost function to evaluate the estimation accuracy as below:

$$\lambda \quad = \quad (\frac{\hat{f}_{h1}(t-1) - \hat{f}_{h1}(t)}{\dot{x}_1(t)} - \frac{f_{h1}(t-1) - f_{h1}(t)}{\dot{x}_1(t)})^2. \tag{9}$$

Remark 1: $\frac{f_{h1}(t-1)-f_{h1}(t)}{\dot{x}_1(t)}$ can be regarded as K_h according to (5), so we can use (9) to evaluate the estimation accuracy of K_h. f_{h1} and $\dot{x}_1$ can be measured by force and velocity sensors, respectively.

Remark 2: Similar idea has been used in [75] for estimating human stiffness in real-time. The estimated stiffness of the human operator's arm has been calculated from the equation: $\triangle F_{est}(t) = K_H \triangle p_{est}(t)$, where $\triangle p_{est}(t) = p_R(t) - p_R(t - t_S)$ and $\triangle F_{est}(t) = F_R(t) - F_R(t - t_S)$. $F_R(t)$ is measured force and $p_R(t)$ is the position of the end-effector, $\triangle F_{est}(t)$ and $\triangle p_{est}(t)$ denote difference of force and position, and t_S is the time step. A recursive identification method using digital filter has been utilized to estimate stiffness parameters in real-time.

We assume that $\frac{f_{h1}(t-1)-f_{h1}(t)}{\dot{x}_1(t)}$ follows the Gaussian distribution, so the random variable set κ_1 of $\frac{f_{h1}(t-1)-f_{h1}(t)}{\dot{x}_1(t)}$ obeys the following distribution:

$$\kappa_1 \sim N(\mu, \sigma^2), \tag{10}$$

where $N(*)$ denotes the Gaussian distribution function, μ denotes the mathematical expectation, and σ^2 denotes the variance of random variable set κ_1. Regarding that the actual human stiffness parameter K_{h1} can be deemed as μ, we can estimate K_{h1} according to Bayesian parameter estimation method if σ^2 is known to the control designer. We rewrite the cost function (9) as follows

$$\lambda \quad = \quad (\hat{\mu} - \mu)^2, \tag{11}$$

where $\hat{\mu}$ is the estimate of μ. We can obtain the predictor probability distribution of stiffness parameter $p(\mu)$ as follows

$$p(\mu) \sim N(\mu_0, \sigma_0^2), \tag{12}$$

where μ_0, σ_0^2 denote predictor expectation and variance of μ, and their values can be found based on the literature about human stiffness measurement [76]. We can obtian the updater probability distribution $p(\mu \mid \kappa)$ as follows

$$p(\mu \mid \kappa) = \frac{p(\kappa \mid \mu)p(\mu)}{\int p(\kappa \mid \mu)p(\mu)d\mu}, \tag{13}$$

where $p(\kappa \mid \mu)$ denotes the joint probability distribution, and it can be calculated as

$$p(\kappa \mid \mu) = \prod_{i=1}^{n} p(\frac{f_{h1i}(t-1) - f_{h1i}(t)}{\dot{x}_{1i}(t)} \mid \mu), \tag{14}$$

where $\frac{f_{h1i}(t-1)-f_{h1i}(t)}{\dot{x}_{1i}(t)}$ is the i-th element of a set κ. Substituting (12), (14) to (13), we can obtain the updater probability distribution $p(\mu \mid \kappa)$ as follows

$$p(\mu \mid \kappa) = \alpha p(\kappa \mid \mu)p(\mu), \tag{15}$$

where α is introduced to absorb the irrelevant terms about μ. Considering that $p(\kappa \mid \mu)$ and $p(\mu)$ follow the Gaussian distribution, we can rewrite (15) as

$$\begin{aligned} p(\mu \mid \kappa) &= \alpha \prod_{i=1}^{n} \frac{1}{\sqrt{2\pi}\sigma} \exp(-\frac{1}{2}\frac{(\frac{f_{h1i}(t-1)-f_{h1i}(t)}{\dot{x}_{1i}(t)} - \mu)^2}{\sigma^2}) \\ &\quad \frac{1}{\sqrt{2\pi}\sigma_0}\exp(-\frac{1}{2}\frac{(\mu-\mu_0)^2}{\sigma_0^2}) \\ &= \alpha_1 \exp(-\frac{1}{2}(\sum_{i=1}^{n} \frac{(\frac{f_{h1i}(t-1)-f_{h1i}(t)}{\dot{x}_{1i}(t)} - \mu)^2}{\sigma^2} \\ &\quad + \frac{(\mu-\mu_0)^2}{\sigma_0^2})) \\ &= \alpha_2 \exp(-\frac{1}{2}((\frac{n}{\sigma^2} + \frac{1}{\sigma_0^2})\mu^2 \\ &\quad -2(\frac{1}{\sigma^2}\sum_{i=1}^{n}\frac{f_{h1i}(t-1) - f_{h1i}(t)}{\dot{x}_{1i}(t)} + \frac{\mu_0}{\sigma_0^2})\mu) \end{aligned} \tag{16}$$

where α_1 and α_2 are parameters used to absorb the irrelevant items of μ. Note that $p(\mu \mid \kappa)$ follows the Gaussian distribution, so we can conclude that

$$p(\mu \mid \kappa) = \frac{1}{\sqrt{2\pi}\sigma_n}\exp(-\frac{1}{2}\frac{(\mu-\mu_n)^2}{\sigma_n^2}) \sim N(\mu_n, \sigma_n^2). \tag{17}$$

Because the coefficient in exponential term in (17) equals its counterpart in (16), we can obtain

$$\begin{aligned} \frac{1}{\sigma_n^2} &= \frac{n}{\sigma^2} + \frac{1}{\sigma_0^2} \\ \frac{\mu_n}{\sigma_n^2} &= \frac{n}{\sigma^2}\hat{\mu}_n + \frac{\mu_0}{\sigma_0^2}, \end{aligned} \tag{18}$$

where

$$\hat{\mu}_n = \frac{1}{n}\sum_{i=1}^{n}\frac{f_{h1i}(t-1) - f_{h1i}(t)}{\dot{x}_{1i}(t)}. \tag{19}$$

We can conclude that

$$\begin{aligned} \mu_n &= \frac{n\sigma_0^2}{n\sigma_0^2 + \sigma^2}\hat{\mu}_n + \frac{\sigma^2}{n\sigma_0^2 + \sigma^2}\mu_0 \\ \sigma_n^2 &= \frac{\sigma^2\sigma_0^2}{n\sigma_0^2 + \sigma^2}. \end{aligned} \tag{20}$$

If we use the quadratic cost function like (9), the Bayesian parameter estimation $\hat{\mu}$ can be described as the conditional expectation when κ is given and μ can be estimated as follows

$$\begin{aligned} \hat{\mu} &= \int \mu p(\mu \mid \kappa)d\mu = \int \mu \frac{1}{\sqrt{2\pi}\sigma_n}\exp(-\frac{1}{2}\frac{(\mu-\mu_n)^2}{\sigma_n^2})d\mu \\ &= \mu_n. \end{aligned} \tag{21}$$

Thus, the Bayesian estimation of μ can be rewritten as:

$$\begin{aligned} \hat{\mu} &= \frac{n\sigma_0^2}{n\sigma_0^2 + \sigma^2}\hat{\mu}_n + \frac{\sigma^2}{n\sigma_0^2 + \sigma^2}\mu_0 \\ &\quad (\hat{\mu}_n = \frac{1}{n}\sum_{i=1}^{n}\frac{f_{h1i}(t-1) - f_{h1i}(t)}{\dot{x}_{1i}(t)}), \\ \hat{\sigma}^2 &= \sigma_n^2 = \frac{\sigma^2\sigma_0^2}{n\sigma_0^2 + \sigma^2}. \end{aligned} \tag{22}$$

From (22) we can conclude that the estimate of human stiffness parameter $\hat{K}_{h1}$ remains in the interval from $(\hat{\mu} - \hat{\sigma})$ to $(\hat{\mu} + \hat{\sigma})$, i.e.,

$$\begin{aligned} K_{h1\min} &= \hat{\mu} - \hat{\sigma}, \\ K_{h1\max} &= \hat{\mu} + \hat{\sigma}. \end{aligned} \tag{23}$$

Then, we can obtain the corresponding human motion intention estimate $\hat{x}_{h1}$ as follows

$$\hat{x}_{h1} \in (\frac{f_{h1}}{K_{h1\max}} + x_1, \frac{f_{h1}}{K_{h1\min}} + x_1). \tag{24}$$

Since $\hat{K}_{h1}$ obeys Gausian distribution, the corresponding human motion intention estimate $\hat{x}_{h1}$ also obeys Gausian distribution, i.e.,

$$\hat{x}_{h1} \sim N(\mu_x, \sigma_x^2), \tag{25}$$

where μ_x and σ_x are the expectation and the variance of $\hat{x}_{h1}$, respectively. They can be described as

$$\begin{aligned} \mu_x &= \frac{f_{h1}}{K_{h1\max}} + x_1 + \frac{\frac{f_{h1}}{K_{h1\min}} - \frac{f_{h1}}{K_{h1\max}}}{2}, \\ \sigma_x &= \frac{\frac{f_{h1}}{K_{h1\min}} - \frac{f_{h1}}{K_{h1\max}}}{2}, \end{aligned} \tag{26}$$

where x_1 denotes the position in one dimension.

Along with increasing n, $\hat{\sigma}$ converges to a small value, and $\hat{\mu}$ converges to $\hat{\mu}_n$. μ_x converges to $\frac{f_{h1}}{\hat{\mu}_n} + x_1$ and σ_x converges to zero. Using this method we can estimate K_{h1} and x_{h1} in one dimension. In a similar way, human stiffness matrix $\hat{K}_h$ and motion intention vector $\hat{x}_h$ can be obtained by Bayesian parameter estimation.

IV. Control Design

After $\hat{x}_h$ and $\hat{K}_h$ are obtained, we set x_d as $\hat{x}_h$, and set K_d as $\hat{K}_h$ to achieve the task objective. We set D_d as $D_d = \mathrm{diag}[\ell\sqrt{K_{d1}}, \ell\sqrt{K_{d2}}, ..., \ell\sqrt{K_{dn}}]$, where ℓ denotes a proper

coefficient between 0 and 1. We set inertia matrix Λ_d close to the robot's inertia matrix M_r. According to (6), we construct the error signal ϖ as

$$\begin{aligned}\varpi &= \Lambda_d(\ddot{x}_d - \ddot{x}) + D_d(\dot{x}_d - \dot{x}) + K_d(x_d - x) + f_r \\ &= \Lambda_d\ddot{e} + D_d\dot{e} + K_d e + f_r, \end{aligned} \tag{27}$$

where $e = x_d - x$, and if we want to achieve the relationship in (6), we should make ϖ converge to zero. To facilitate analysis, we define another impedance error ω as

$$\omega = K_f\varpi = \ddot{e} + K_c\dot{e} + K_k e + K_f f_r \tag{28}$$

where $K_f = \Lambda_d^{-1}$, $K_c = \Lambda_d^{-1}D_d$, $K_k = \Lambda_d^{-1}K_d$. We choose two positive-definite matrices A and B as

$$\begin{aligned} A + B &= K_c \\ \dot{A} + BA &= K_k. \end{aligned} \tag{29}$$

And we define

$$\dot{f}_{rl} + Bf_{rl} = K_f f_r. \tag{30}$$

According to (29) and (30), we rewrite (28) as

$$\omega = \ddot{e} + (A + B)\dot{e} + (\dot{A} + AB)e + \dot{f}_{rl} + Bf_{rl}. \tag{31}$$

Similar in [77], we define an auxiliary variable z as

$$z = \dot{e} + Ae + f_{rl}, \tag{32}$$

so we can rewrite (31) as

$$\omega = \dot{z} + Bz. \tag{33}$$

When z converges to zero, we can conclude that $\dot{z} \to 0$ if its limit exists. We define a virtual state variable vector x_r as

$$\dot{x}_r = \dot{x}_d + Ae + f_{rl}, \tag{34}$$

so z can be rewritten as

$$z = \dot{x}_r - \dot{x}, \tag{35}$$

In the following, we employ z to design an impedance controller and analyze control stability.

Consider the following Lyapunov function candidate as

$$V_1 = \frac{1}{2}z^T M_r(x)z. \tag{36}$$

Differentiating V_1 with respect to time, we have

$$\dot{V}_1 = \frac{1}{2}z^T\dot{M}_r(x)z + z^T M_r(x)\dot{z}, \tag{37}$$

matrix $\theta^T(2C_r(x,\dot{x}) - \dot{M}_r(x))\theta = 0, \forall\theta \in R^n$, where $(2C_r(x,\dot{x}) - \dot{M}_r(x))$ is skew-symmetric. Thus, we can rewrite $\dot{V}_1$ as

$$\dot{V}_1 = z^T C_r(x,\dot{x})z + z^T M_r(x)\dot{z}. \tag{38}$$

Considering (35), we rewrite (1) as

$$M_r(x)\dot{z} + C_r(x,\dot{x})z = -u - f_r + M_r\ddot{x}_r + C_r\dot{x}_r + G_r, \tag{39}$$

so $\dot{V}_1$ can be written as

$$\dot{V}_1 = z^T(-u - f_r + M_r\ddot{x}_r + C_r\dot{x}_r + G_r), \tag{40}$$

and the model-based impedance controller u can be designed as

$$u = K_g z + M_r\ddot{x}_r + C_r\dot{x}_r + G_r - f_r. \tag{41}$$

Where K_g is a positive definite matrix, when u is designed as (41), we can obtain

$$\dot{V}_1 = -z^T K_g z < 0. \tag{42}$$

To address uncertainties in robot's dynamic model, i.e., $M_r(x)$, $C_r(x,\dot{x})$ and $G_r(x)$ are unknown in practical situations, an adaptive impedance control is designed in this part. The adaptive law is designed as

$$\dot{\hat{W}}_i = -\Gamma_i[S_i(Z_i)z_i + \delta_i\hat{W}_i], i = 1, 2, ..., n, \tag{43}$$

where $\hat{W}_i$ is the weight estimate of NN, $\Gamma_i = \Gamma_i^T$ is a positive gain matrix and δ_i is a small positive constant which is used to improve the system robustness. Z_i=[x^T, $\dot{x}^T$, $\dot{x}_r^T$, $\ddot{x}_r^T$] is the input of NN. $\hat{W}^T S(Z)$ is used to estimate $W^{*T}S(Z)$ as below

$$W^{*T}S(Z) = M_r\ddot{x}_r + C_r\dot{x}_r + G_r - \epsilon(Z), \tag{44}$$

where W_i^* is the actual weight of NN, $S(Z)$ denotes the basis function, the estimation error $\epsilon(Z)$ stays in bounds over the compact set Ω, $\forall Z \in \Omega$, $||\epsilon(Z)|| < \bar{\epsilon}$, with $\bar{\epsilon}$ as a positive constant.

Assumption 1 [78]: There exist ideal weight vectors W^* such that $|\epsilon(Z)| \leq \bar{\epsilon}$ with constant $\bar{\epsilon} > 0$ for all $Z \in \Omega_Z$.

The NN impedance controller can be designed as

$$u = K_g z + \hat{W}^T S(Z) - f_r. \tag{45}$$

We consider another Lyapunov function V_2 candidate as

$$V_2 = \frac{1}{2}z^T M_r(x)z + \frac{1}{2}\sum_{i=1}^{n}\tilde{W}_i^T\Gamma_i^{-1}\tilde{W}_i. \tag{46}$$

We define the weight error $\tilde{W}_i = \hat{W}_i - W_i^*$. Differentiating V_2 with respect to time, we have

$$\begin{aligned}\dot{V}_2 &= z^T(u + f_r - (M_r\ddot{x}_r + C_r\dot{x}_r + G_r)) \\ &\quad + \sum_{i=1}^{n}\tilde{W}_i^T\Gamma_i^{-1}\dot{\hat{W}}_i. \end{aligned} \tag{47}$$

Substituting (45) to (47), we can obtain

$$\begin{aligned}\dot{V}_2 &= z^T(-K_g z + \hat{W}^T S(Z) - f_r + f_r - (M_r\ddot{x}_r \\ &\quad + C_r\dot{x}_r + G_r)) + \sum_{i=1}^{n}\tilde{W}_i^T\Gamma_i^{-1}\dot{\hat{W}}_i, \end{aligned} \tag{48}$$

Substituting (43) to (48), we have

$$\begin{aligned}\dot{V}_2 &= z^T(-K_g z + \hat{W}^T S(Z) - W^{*T}S(Z) - \epsilon(Z)) \\ &\quad + \sum_{i=1}^{n}\tilde{W}_i^T\Gamma_i^{-1}\{-\Gamma_i[S_i(Z_i)z_i + \delta_i\hat{W}_i]\} \\ &= -z^T K_g z + z^T\hat{W}^T S(Z) - z^T W^{*T}S(Z) - z^T\epsilon(Z) \\ &\quad - \sum_{i=1}^{n} z_i\tilde{W}_i^T S_i(Z_i) + \sum_{i=1}^{n}\tilde{W}_i^T\delta_i\hat{W}_i. \end{aligned} \tag{49}$$

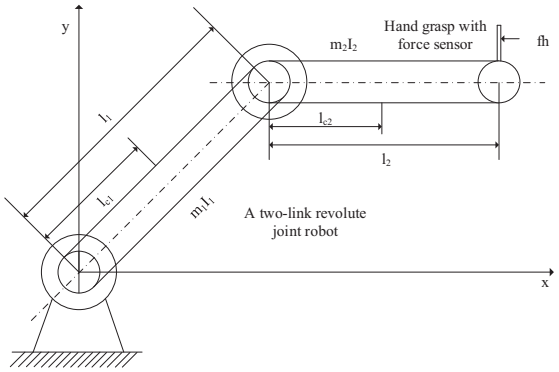

Fig. 3: A two-link revolute joint robot: human partner is holding the handle on its end-effector, and an interaction force is applied to the force sensor.

We can obtain

$$\begin{aligned}\dot{V}_2 &\leq -z^T(K_g - \frac{1}{2}I_{n\times n})z + \frac{1}{2}||\epsilon(Z)||^2 \\ &\quad + \sum_{i=1}^{n}\frac{\delta_i}{2}(||W_i^*||^2 - ||\tilde{W}_i||^2) \\ &\leq -\rho V_2 + C, \end{aligned} \tag{50}$$

where

$$\begin{aligned}\rho &= \min(\min(\frac{2\varsigma_{\min}(K_g - \frac{1}{2}I)}{\varsigma_{\max}(M_r(x))}, \min(\frac{\delta_i}{\varsigma_{\max}(\Gamma_i^{-1})})), \\ C &= \frac{1}{2}||\bar{\epsilon}||^2 + \sum_{i=1}^{n}\frac{\delta_i}{2}||W_i^*||^2. \end{aligned} \tag{51}$$

where ς denotes the eigenvalue of a matrix, $\bar{\epsilon}$ denotes the bound of ϵ. For ensuring $\rho > 0$, we should make $\varsigma_{\min}(K_g - \frac{1}{2}I) > 0$, $\varsigma_{\max}(\Gamma_i^{-1}) > 0$.

Theorem 1: For each compact set Ω_0, the initial conditions z_0 and $\hat{W}_0$ are in bounds, the controller (45) guarantees that the closed-loop error signal z remains in the compact set Ω_z, and the weight error $\tilde{W}$ remains in the compact set $\Omega_{\tilde{W}}$, i.e.,

$$\begin{aligned}\Omega_z &= \{z\epsilon R^n|\ ||z|| \leq \sqrt{\frac{D}{\varsigma_{\min}(M_r(x))}}\} \\ \Omega_W &= \{\tilde{W}\epsilon R^{l\times n}|\ ||\tilde{W}|| \leq \sqrt{\frac{D}{\varsigma_{\min}(\Gamma^{-1})}}\}, \end{aligned} \tag{52}$$

where $D = 2(V_2(0) + C)/\rho$ with positive constants C and ρ is given in (51).

V. Simulation

In this section, we consider a scenario where a human partner is holding hand grasp on robotic end-effector with a force sensor. A two-link revolute joint robot shown in Fig. 3 is considered and an interaction force is applied to the end-effector by the human partner.

In Fig. 3, m_1, m_2 and l_1, l_2 denote the mass and length of link 1, 2, respectively. l_{c1}, l_{c2} denotes the distance from joint 1, 2 to the mass center of link 1, 2, and I_1, I_2 denotes the moment of Inertia of link 1, 2. The simulation parameter values are chosen as: m_1=2.0kg, m_2=0.85kg, l_1=1.40m, l_2=1.24m, l_{c1}=0.70m, l_{c2}=0.62m, I_1=0.980kgm^2, I_2=0.953kgm^2.

In simulations, robot's dynamic model parameter matrices $M(q)$, $C(q,\dot{q})$, $G(q)$ in the joint space in (1) can be calculated as

$$M(q) = \begin{bmatrix} m_{t1} & m_{t2} \\ m_{t3} & r(2) \end{bmatrix} \tag{53}$$

$$C(q,\dot{q}) = \begin{bmatrix} c_{t1} & c_{t2} \\ c_{t3} & 0 \end{bmatrix} \tag{54}$$

$$G(q) = \begin{bmatrix} g_{t1} \\ g_{t2} \end{bmatrix}, \tag{55}$$

where $m_{t1} = r(1) + r(2) + 2r(3)\cos(q(3))$, $m_{t2} = r(2) + r(3)\cos(q(3))$, $m_{t3} = r(2) + r(3)\cos(q(3))$, $c_{t1} = -r(3)q(4)\sin(q(3))$, $c_{t2} = -r(3)(q(2)+q(4))\sin(q(3))$, $c_{t3} = r(3)q(2)\sin(q(3))$, $g_{t1} = r(4)g\cos(q(1)) + r(5)g\cos(q(1) + q(3))$, $g_{t2} = r(5)g\cos(q(1) + q(3))$.

The system state variables $q = [q(1); q(3)]$, $\dot{q} = [q(2); q(4)]$, $q(1)$ and $q(3)$ denote first and second joint angle, respectively, $q(2)$ and $q(4)$ denote first and second joint angular velocity, respectively. The variables $r(1) = m_1 l_{c1}^2 + m_2 l_1^2 + I_1$, $r(2) = m_2 l_{c2}^2 + I_2$, $r(3) = m_2 l_1 l_{c2}$, $r(4) = m_1 l_{c2} + m_2 l_1$ and $r(5) = m_2 l_{c2}$. The Jacobian matrix in (1) can be obtained according to l_1, l_2 and q as follow

$$J = \begin{bmatrix} J_{11} & J_{12} \\ J_{21} & J_{22} \end{bmatrix}, \tag{56}$$

where $J_{11} = -l_1\sin(q(1)) - l_2\sin(q(1) + q(3))$, $J_{12} = -l_2\sin(q(1) + q(3))$, $J_{21} = l_1\cos(q(1)) + l_2\cos(q(1) + q(3))$, $J_{22} = l_2\cos(q(1) + q(3))$.

If $M(q)$, $C(q,q)$, $G(q)$ and J are obtained, we can calculate robot's dynamic parameter matrices in the Cartesian space $M_r(x)$, $C_r(x,\dot{x})$ and $G_r(x)$ in (4).

We consider that a human partner applies interaction force to the hand grasp on the end-effector from initial position [0.85m, 1.05m] at the initial velocity [0m/s, 0m/s] to the target position [0.75m, 0.75m].

A. The estimation of human stiffness and motion intention

We suppose that human's real dynamic model in X-direction can be described as $f_{h1} = -300(x(1) - 0.75)$, where the actual human stiffness in X-direction $K_{h1} = 300$Nm, and human motion intention in X-direction $x_{d1} = 0.75$m. We use Bayesian method to estimate human stiffness K_{h1} in X-direction, and the same method is used for estimating K_{h2} in Y-direction. Firstly, we set a predictor probability distribution of human stiffness parameter $p(\mu_1)$ as follows

$$\begin{aligned} &p(\mu_1) \sim N(200, 10^2), \\ &p(\mu_1) \sim N(200, 15^2), \\ &p(\mu_1) \sim N(100, 10^2), \\ &p(\mu_1) \sim N(400, 10^2). \end{aligned} \tag{57}$$

In the random variable set κ_1 that obeys the distribution $\kappa_1 \sim N(\mu, 10^2)$, using the proposed method in Section III, different predictor probability distributions of human stiffness parameter K_{h1} can be estimated as shown in Fig. 4(a). From

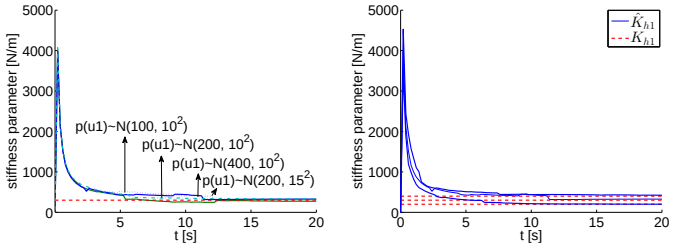

(a) different predictor probability distribution of human stiffness estimation. (b) human stiffness estimations.

Fig. 4: human stiffness estimation and standard deviation in X-direction.

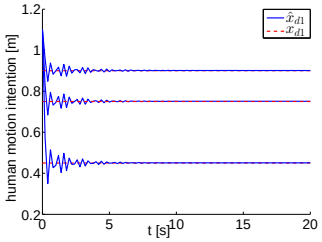

Fig. 5: human motion intention estimation in X-direction.

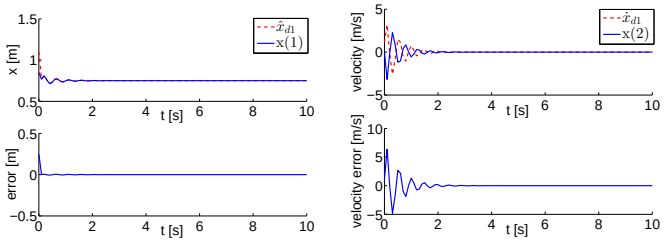

(a) position and error. (b) velocity and velocity error.

Fig. 6: position and velocity value and error in X-direction.

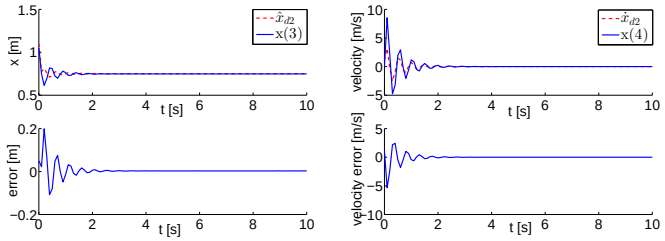

(a) position and error. (b) velocity and velocity error.

Fig. 7: position and velocity value and error in Y-direction.

this figure, we can conclude that K_{h1} can be estimated with different mathematical expectations or different variances of $p(\mu_1)$. In Fig. 4(b), we can see that by setting different stiffness parameters $200\mathrm{N/m}$, $300\mathrm{N/m}$, $400\mathrm{N/m}$, respectively, K_{h1} can be successfully estimated by our proposed method in the same predictor probability distribution of human stiffness parameter.

In Fig. 5(a), human motion intention estimation $\hat{x}_{d1}$ and variance of $\hat{x}_{d1}$ have been obtained by dynamic relationship between x_{d1} and K_{h1}. Different human motion intentions have been set as $0.45\mathrm{m}$, $0.75\mathrm{m}$ and $0.90\mathrm{m}$ when $p(\mu_1) \sim N(200, 10^2)$. We can see that with the proposed method, different human motion intention can be estimated.

B. Impedance control with neural networks

As discussed in Section II, we set the target impedance model as a simplified spring model $f_{r1} = -K_{r1}(x(1) - x_{d1})$, $f_{r2} = -K_{r2}(x(3) - x_{d2})$ for convenient analysis, where $K_{r1} = \hat{K}_{h1}$, $x_{d1} = \hat{x}_{h1}$, $K_{r2} = \hat{K}_{h2}$, $x_{d2} = \hat{x}_{h2}$. We use NN to compensate for uncertainties in control design. The RBFNN centers are chosen in the region of $[-1,1]\times[-1,1]\times[-1,1]\times[-1,1]\times[-1,1]\times[-1,1]\times[-1,1]\times[-1,1]$, the number of NN nodes is chosen as 2^8, and the initial value of NN weight is set as 0. Γ_1 and Γ_2 are selected as $100\boldsymbol{I}$, and δ_i=0.002. And two important matrices A and B are calculated based on (29). In this human-robot interactive process, human's real model is described as $f_{r1} = -300(x(1) - 0.75)$, $f_{r2} = -300(x(3) - 0.75)$, human partner applies interaction force $f_h = [f_{h1}, f_{h2}]$ to the hand grasp on the end-effector from initial position [0.85m, 1.05m] at the initial velocity [0m/s, 0m/s] to the target position [0.75m, 0.75m].

Fig. 6(a) shows the position and the position error in X-direction between $x(1)$ and x_{d1}, Fig. 6(b) shows the velocity and velocity error in X-direction between $x(2)$ and $\dot{x}_{d1}$. Note that when there exists no interaction force, the position error and velocity error will converge to zero according to the dynamical relationship in (6). Fig. 7(a) and Fig. 7(b) show the position and position error, the velocity and velocity error in Y-direction, respectively. Fig. 8(a) shows the tracking performance of velocity $x(2)$ in X-direction, and Fig. 8(b) shows the tracking performance of auxiliary variable z_1 in X-direction. We can conclude that under the proposed method, the error signal ϖ converges to zero. Fig. 9 shows the interaction force between human and object f_{r1} in X-direction.

VI. Experiment

In this section, we consider a scenario where an interaction force is applied to the arm of a robotic manipulator by a human partner. We use the S_0 shoulder joint on the right arm of dual-

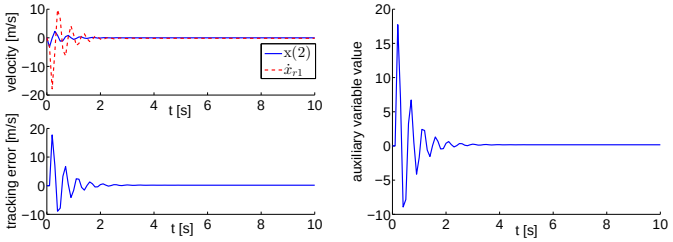

(a) velocity $x(2)$ and virtual state variable $\dot{x}_{r1}$. (b) auxiliary variable z

Fig. 8: tracking performance in X-direction.

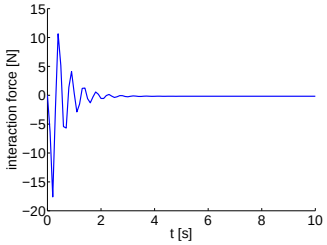

Fig. 9: interaction force in X-direction.

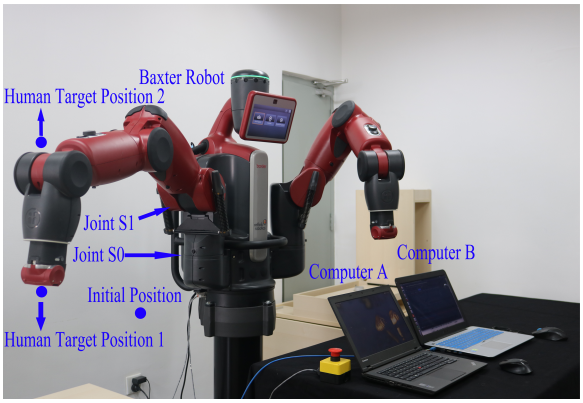

Fig. 10: Baxter® robot experimental platform: there are two computers and one Baxter® robot.

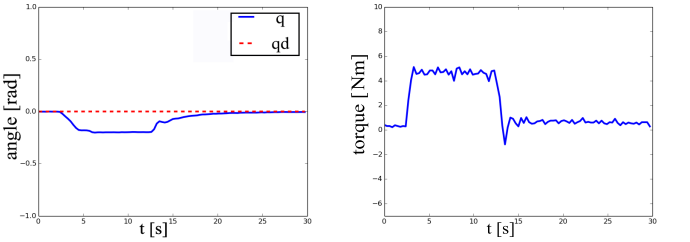

(a) angle with a target angle of 0.2rad. (b) interaction torque with a target angle of 0.2rad.

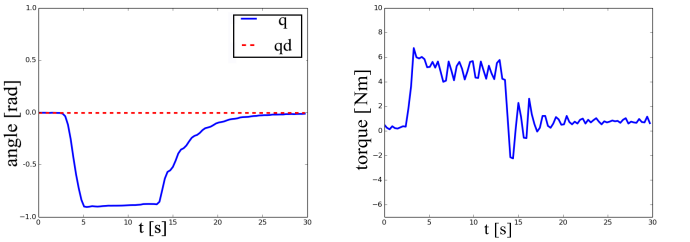

(c) angle with a target angle of 0.8rad. (d) interaction torque with a target angle of 0.8rad.

Fig. 12: angle and interaction torque when human moves the robot to 0.2rad and 0.8rad considering that the human motion intention and stiffness estimation are not involved.

arm humanoid robot Baxter® in our experiment. A human robot interactive experiment is developed to prove the validity of our proposed control method.

A. Experiment settings

Baxter® robot has torque sensors in every joint of both two arms. Angle, angle velocity and torque information can be read from its dedicated controller. Seen from Fig. 10, there are two computers (A and B) for controlling robot and calculation in this experiment. Computer A is used to calculate the neural network compensation by Matlab Simulink® and transform the compensation value to the computer B by UDP. Computer B is used to receive the robot state signals and generate control signal to control the robot by Baxter Robot Operating System SDK (RSDK) in Ubuntu 14.04 LTS. We rewrite the target impedance model in joint space as $\tau_{f_r} = K_{S_0}(x - x_d)$, and we consider human impedance model in joint space as $\tau_{f_h} = K_h(x - x_h)$. K_{S_0}, K_h denote S_0 and human joint stiffness parameter, respectively and x_h denotes the human target angle, x denotes the current angle, and τ_{f_h} denotes the interaction torque.

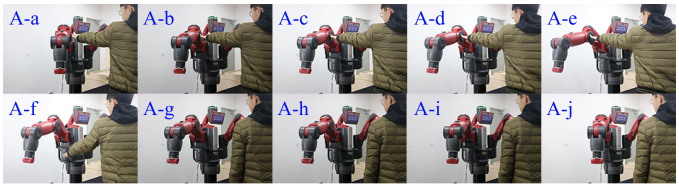

(a) the experimental results of impedance control without estimation: seen from A-a to A-e, a human partner operates the robot to the target position 1; seen from A-f to A-j, the interaction torque disappears and the robot moves back to the initial position.

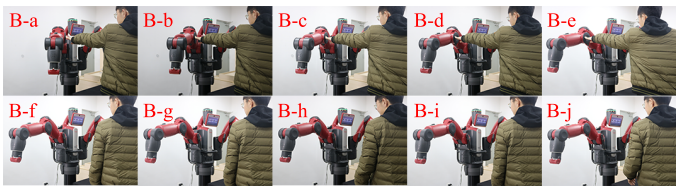

(b) the experimental results of impedance control with human motion intention estimation: seen from B-a to B-e, a human partner operates the robot to the target position 1; seen from B-f to B-j, the interaction torque disappears and the robot still remains in the current position.

Fig. 11: the experimental results.

B. Case 1. No estimation

In this part, we consider a scenario that a human partner operates S_0 shoulder joint of Baxter® robot's right arm to the human target angle. We design robot target impedance stiffness parameter K_{S_0} as 3Nm/rad, but different human target angles x_h: 0.2rad and 0.8rad. Fixed desired angle x_d of robot is considered in this experiment and the robot initial position is set as 0rad. An interaction force is applied to the robot arm from 3s to 13s. Seen from Fig. 11(a), the robot moves from 0rad to 0.5rad driven by human partner and back to 0rad under the impedance control method. Fig. 12 shows that when K_{S_0} is fixed, the interaction torques have proportional relationships with the error between current angle x and desired angle x_d. Larger error between current position and x_d will generate greater interaction torque.

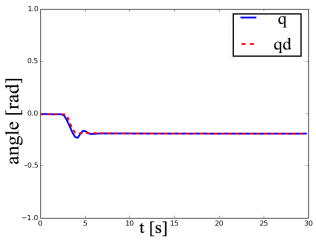

(a) angle with a target angle of 0.2rad.

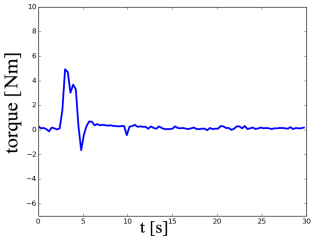

(b) interaction torque with a target angle of 0.2rad.

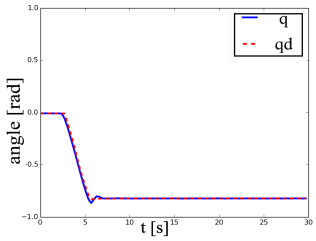

(c) angle with a target angle of 0.8rad.

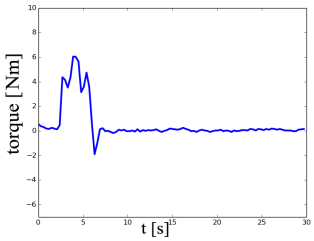

(d) interaction torque with a target angle of 0.8rad.

Fig. 13: angle and interaction torque when human moves the robot to 0.2rad and 0.8rad considering that the human motion intention estimation is involved.

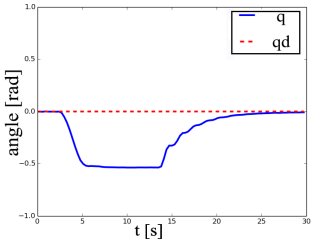

(a) angle without human motion intention estimation.

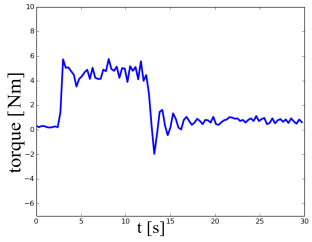

(b) interaction torque without human motion intention estimation.

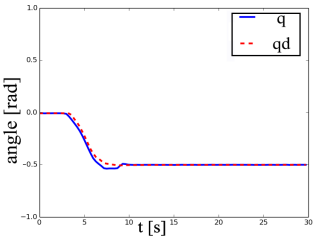

(c) angle with Bayesian estimation method.

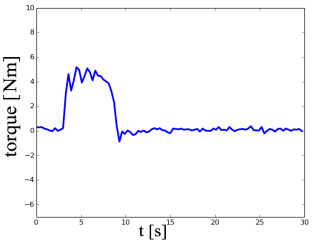

(d) interaction torque with Bayesian estimation method.

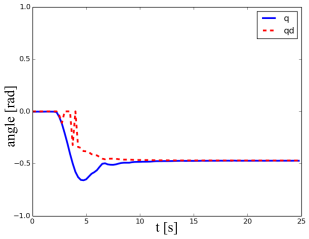

(e) angle with NN estimation method.

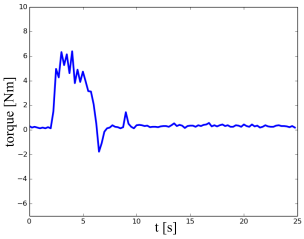

(f) interaction torque with NN estimation method.

Fig. 14: angle and interaction torque when human moves the robot to 0.5rad.

C. Case 2. Motion intention estimation

Motion intention estimation $\hat{x}_d$ is involved in this part. In Fig. 11(b), the robot moves from initial angle 0rad to target angle of 0.5rad driven by human partner, an interaction torque is applied to the robot arm from 3s to 8s, and the robot will remain the current angle after 8s when motion intention estimation based on Bayesian esitmated method is involved. Fig. 13 shows relationships between the interaction torques and $x - x_d$ when human moves robot to 0.2rad and 0.8rad. As can be seen from Fig. 14(b) and 14(d), we can conclude that the interaction torque under our proposed method is smaller than the torque under impedance control when motion intention estimation is not involved. And the robot will remain in the position when interaction torque disappears as can be seen Fig. 14(c). In this part, we also utilize NN method to estimate human motion intention for comparison with our proposed method. Indicated from Fig. 14(e), the convergence of NN estimation method is slower than our proposed Bayesian estimation method. NNs rely on online sensor information which will bring heavy computational burden to influence convergence.

D. Case 3. Impedance estimation

In this part, the target angle impedance stiffness value is set as $3\mathrm{Nm/rad}$ and $15\mathrm{Nm/rad}$, respectively. The experiment process is same as the process in Case 1. Indicated from Fig. 15, we can see the proportional relationships with $\hat{K}_h$ and interaction torque, i.e., larger stiffness will generate greater interaction torque at the same angle displacement. We also consider the human stiffness estimation based on Bayesian method in Fig. 16, from which we can conclude that the joint stiffness can be estimated by our proposed method. In Fig. 17, we set the predictor probability distribution of joint stiffness parameter as $p(\mu) \sim N(1, 0.1^2), N(5, 0.1^2)$, respectively. Joint stiffness can be estimated successfully considering different probability distributions of human stiffness parameter.

E. Case 4. Simultaneous estimations

In this part, we use Bayesian method to estimate joint stiffness and human target angle simultaneously, where the predictor probability distribution of stiffness parameter $p(\mu)$ is set as $p(\mu) \sim N(1, 0.1^2)$. The experiment process is divided into two phases. In the first phase it is the same as the process (S_0 joint) in Case 2, where human partner moves the robot to the target position 1. In the second phase, we utilize the joint S_1 to lift the robot to the target position 2. The mean and standard deviation of the above measures are computed using 50 data points (10 human subjects $\times$ 5 repetitions). Each of 10 human subjects (P1, P2, ..., and P10) repeats the task for 5 times (T1, T2, T3, T4 and T5). Indicated from Fig. 18, we

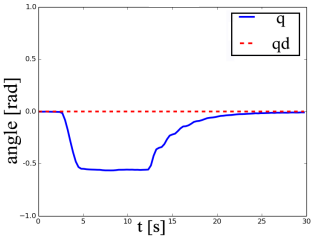

(a) angle when K=3Nm/rad.

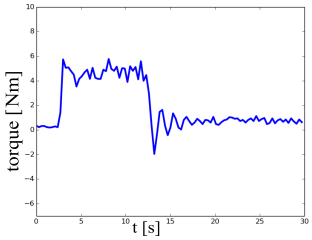

(b) interaction torque when K=3Nm/rad.

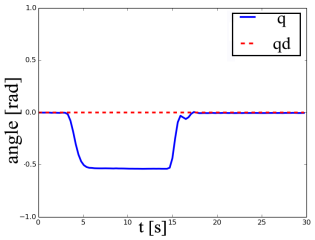

(c) angle with when K=15Nm/rad.

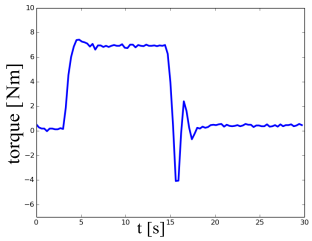

(d) interaction torque when K=15Nm/rad.

Fig. 15: angle and interaction torque when K=3Nm/rad, 15Nm/rad, respectively.

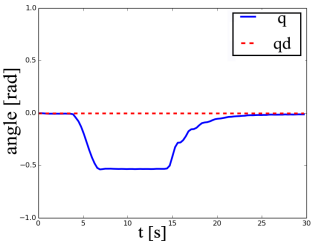

(a) angle when K is estimated.

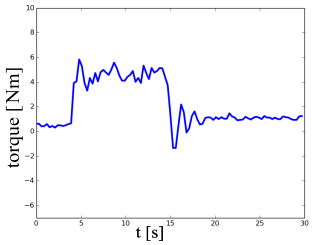

(b) interaction torque when K is estimated.

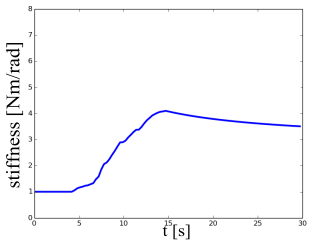

(c) K estimation.

Fig. 16: angle, interaction torque and stiffness estimation when K is estimated.

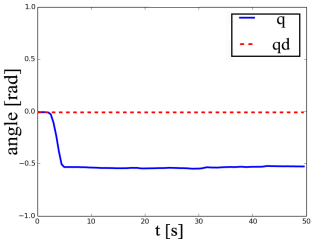

(a) angle when predictor probability distribution $p(\mu) \sim N(1, 0.1^2)$.

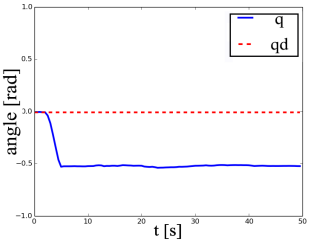

(b) angle when predictor probability distribution $p(\mu) \sim N(5, 0.1^2)$.

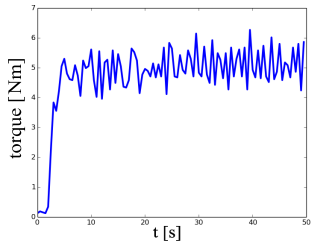

(c) interaction torque when predictor probability distribution $p(\mu) \sim N(1, 0.1^2)$.

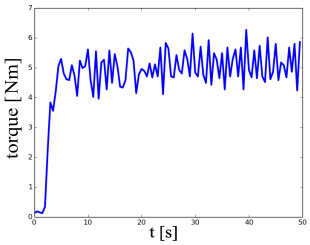

(d) interaction torque when predictor probability distribution $p(\mu) \sim N(5, 0.1^2)$.

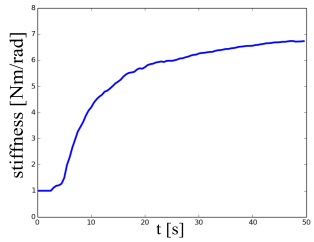

(e) estimated stiffness when predictor probability distribution $p(\mu) \sim N(1, 0.1^2)$.

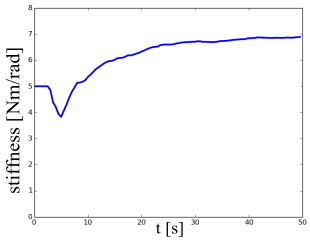

(f) estimated stiffness when predictor probability distribution $p(\mu) \sim N(5, 0.1^2)$.

Fig. 17: angle, interaction torque and estimated stiffness when predictor probability distribution $p(\mu) \sim N(1, 0.1^2), N(5, 0.1^2)$, respectively.

can see that both human motion intention and joint stiffness can be estimated successfully, which show the robustness of the proposed method. We provide statistical analysis of estimated stiffness of one human subject for 5 repetitions when interacting with the robot's S_0 and S_1 joints. Indicated from Figs. 18(b) and 18(d), we can see that all estimated stiffness parameters converge to a constant value. Table 1 shows that the convergence values are "$8.78 \pm 0.13\mathrm{Nm/rad}$" and "$9.33 \pm 0.11\mathrm{Nm/rad}$" in S_0 and S_1 joints, respectively. In Table 2, we can find that the stiffness of 10 human subjects can be estimated successfully, and all estimated parameters converge to constant values in reasonable times.

And the experimental results in a 7-degree-of-freedom are shown in Fig. 19, the proposed controller and Bayesian estimation method are utilized in this task. Experiment results on a Baxter® robot platform illustrate good performance.

TABLE I: estimated stiffness value for human subject P1 when interacting with robotic joints S_0 and S_1 for 5 repetitions (T1-T5).

repetition	S_0 value (Nm/rad)	S_1 value (Nm/rad)
T1	8.67	9.33
T2	8.71	9.21
T3	8.78	9.19
T4	9.02	9.46
T5	8.70	9.45
mean	8.78	9.33
standard deviation	0.13	0.11

TABLE II: convergence mean time (within the 10 percent range of convergence value) and stiffness value when human subjects (P1-P10) interacting with robotic joint S_0.

human subject	mean time (s)	stiffness (Nm/rad)
P1	15.10	8.78 ± 0.13
P2	6.28	6.47 ± 0.16
P3	7.50	10.19 ± 0.23
P4	11.25	13.23 ± 0.26
P5	5.25	5.78 ± 0.14
P6	4.50	7.92 ± 0.21
P7	10.25	15.32 ± 0.26
P8	9.75	8.32 ± 0.12
P9	5.75	9.93 ± 0.20
P10	6.08	7.28 ± 0.18

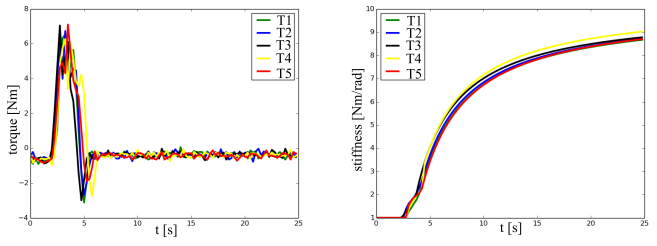

(a) interaction torques in joint S_0.

(b) estimated stiffness in joint S_0.

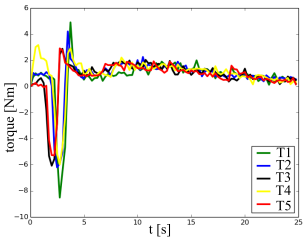

(c) interaction torques in joint S_1.

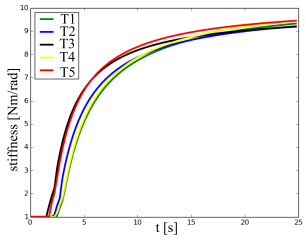

(d) estimated stiffness in joint S_1.

Fig. 18: interaction torque and estimated stiffness when human subject P1 interacting with robotic joint S_0 and S_1 for 5 repetitions when predictor probability distribution $p(\mu) \sim N(1, 0.1^2)$.

Fig. 19: 7-degree-of-freedom experiment.

VII. Conclusion

In this paper, a Bayesian method has been proposed to estimate human impedance and motion intention in a human-robot collaborative task. Estimated stiffness obeying Gaussian distribution has been obtained by Bayesian estimation combining with prior knowledge of human stiffness. According to the dynamic relationship, human motion intention can be also estimated. NNs have been used to compensate for uncertainties in robotic dynamics and an adaptive impedance control strategy has been employed to track a target impedance model. Comparative simulation and experimental results have been carried out to verify advantages of the proposed control strategy and the effectiveness of estimation method.

References

[1] H. Qiao, M. Wang, J. Su, S. Jia, and R. Li, "The concept of attractive region in environment and its application in high-precision tasks with low-precision systems," *IEEE/ASME Transactions on Mechatronics*, vol. 20, no. 5, pp. 2311–2327, 2015.

[2] Z. Li, Y. Kang, Z. Xiao, and W. Song, "Human–robot coordination control of robotic exoskeletons by skill transfers," *IEEE Transactions on Industrial Electronics*, vol. 64, no. 6, pp. 5171–5181, 2017.

[3] M. Chen, S.-Y. Shao, and B. Jiang, "Adaptive neural control of uncertain nonlinear systems using disturbance observer," *IEEE Transactions on Cybernetics*, vol. 47, no. 10, pp. 3110–3123, 2017.

[4] Z. Li, B. Huang, Z. Ye, M. Deng, and C. Yang, "Physical human-robot interaction of a robotic exoskeleton by admittance control," *IEEE Transactions on Industrial Electronics*, vol. 65, no. 12, pp. 9614–9624, 2018.

[5] J. Baraglia, M. Cakmak, Y. Nagai, R. P. Rao, and M. Asada, "Efficient human-robot collaboration: when should a robot take initiative?," *The International Journal of Robotics Research*, vol. 36, no. 5-7, pp. 563–579, 2017.

[6] P. Maurice, M. E. Huber, N. Hogan, and D. Sternad, "Velocity-curvature patterns limit human–robot physical interaction," *IEEE Robotics and Automation Letters*, vol. 3, no. 1, pp. 249–256, 2018.

[7] Y. Cheng, Y. Wang, H. Yu, Y. Zhang, J. Zhang, Q. Yang, H. Sheng, and L. Bai, "Solenoid model for visualizing magnetic flux leakage testing of complex defects," *NDT & E International*, vol. 100, pp. 166–174, 2018.

[8] W. He, W. Ge, Y. Li, Y.-J. Liu, C. Yang, and C. Sun, "Model identification and control design for a humanoid robot," *IEEE Transactions on Systems, Man, and Cybernetics: Systems*, vol. 47, no. 1, pp. 45–57, 2017.

[9] H. Modares, I. Ranatunga, F. L. Lewis, and D. O. Popa, "Optimized assistive human–robot interaction using reinforcement learning," *IEEE Transactions on Cybernetics*, vol. 46, no. 3, pp. 655–667, 2016.

[10] M. Gombolay, A. Bair, C. Huang, and J. Shah, "Computational design of mixed-initiative human–robot teaming that considers human factors: situational awareness, workload, and workflow preferences," *The International Journal of Robotics Research*, vol. 36, no. 5-7, pp. 597–617, 2017.

[11] B. Gao, X. Li, W. L. Woo, and G. yun Tian, "Physics-based image segmentation using first order statistical properties and genetic algorithm for inductive thermography imaging," *IEEE Transactions on Image Processing*, vol. 27, no. 5, pp. 2160–2175, 2018.

[12] D. Liu, Y. Xu, Q. Wei, and X. Liu, "Residential energy scheduling for variable weather solar energy based on adaptive dynamic programming," *IEEE/CAA Journal of Automatica Sinica*, vol. 5, no. 1, pp. 36–46, 2018.

[13] Q. Zhou, H. Li, L. Wang, and R. Lu, "Prescribed performance observer-based adaptive fuzzy control for nonstrict-feedback stochastic nonlinear systems," *IEEE Transactions on Systems, Man, and Cybernetics: Systems*, vol. 48, no. 10, pp. 1747–1758, 2018.

[14] C. Sun and Y. Xia, "An analysis of a neural dynamical approach to solving optimization problems," *IEEE Transactions on Automatic Control*, vol. 54, no. 8, pp. 1972–1977, 2009.

[15] B. Luo, H.-N. Wu, and H.-X. Li, "Adaptive optimal control of highly dissipative nonlinear spatially distributed processes with neuro-dynamic programming," *IEEE Transactions on Neural Networks and Learning Systems*, vol. 26, no. 4, pp. 684–696, 2015.

[16] G. Wu, J. Sun, and J. Chen, "Optimal linear quadratic regulator of switched systems," *IEEE Transactions on Automatic Control*, vol. 64, no. 7, pp. 2898–2904, 2019.

[17] N. Hogan, "Impedance control: An approach to manipulation," *Journal of Dynamic Systems, Measurement, and Control*, vol. 107, no. 1, pp. 8–16, 1985.

[18] S. Jung and T. Hsia, "Neural network impedance force control of robot manipulator," *IEEE Transactions on Industrial Electronics*, vol. 45, no. 3, pp. 451–461, 1998.

[19] W.-S. Lu and Q.-H. Meng, "Impedance control with adaptation for robotic manipulations," *IEEE Transactions on Robotics and Automation*, vol. 7, no. 3, pp. 408–415, 1991.

[20] F. Ficuciello, L. Villani, and B. Siciliano, "Variable impedance control of redundant manipulators for intuitive human–robot physical interaction," *IEEE Transactions on Robotics*, vol. 31, no. 4, pp. 850–863, 2015.

[21] Y. Song and X. Yuan, "Low-cost adaptive fault-tolerant approach for semiactive suspension control of high-speed trains," *IEEE Transactions on Industrial Electronics*, vol. 63, no. 11, pp. 7084–7093, 2016.

[22] S. Haddadin and E. Croft, "Physical human–robot interaction," in *Springer Handbook of Robotics*, pp. 1835–1874, Springer, 2016.

[23] D. P. Losey and M. K. OMalley, "Trajectory deformations from physical human–robot interaction," *IEEE Transactions on Robotics*, vol. 34, no. 1, pp. 126–138, 2018.

[24] Z. Ju and H. Liu, "Human hand motion analysis with multisensory information," *IEEE/AsMe Transactions on Mechatronics*, vol. 19, no. 2, pp. 456–466, 2014.

[25] Y. Li and S. S. Ge, "Human-robot collaboration based on motion intention estimation," *IEEE/ASME Transactions on Mechatronics*, vol. 19, pp. 1007–1014, June 2014.

[26] R. B. Warrier and S. Devasia, "Iterative learning from novice human demonstrations for output tracking," *IEEE Transactions on Human-Machine Systems*, vol. 46, pp. 510–521, Aug 2016.

[27] J. Mainprice, R. Hayne, and D. Berenson, "Goal set inverse optimal control and iterative replanning for predicting human reaching motions in shared workspaces," *IEEE Transactions on Robotics*, vol. 32, no. 4, pp. 897–908, 2016.

[28] B. Corteville, E. Aertbeliën, H. Bruyninckx, J. De Schutter, and H. Van Brussel, "Human-inspired robot assistant for fast point-to-point movements," in *Robotics and Automation, 2007 IEEE International Conference on*, pp. 3639–3644, IEEE, 2007.

[29] Y. Li, K. P. Tee, W. L. Chan, R. Yan, Y. Chua, and D. K. Limbu, "Continuous role adaptation for human–robot shared control," *IEEE Transactions on Robotics*, vol. 31, no. 3, pp. 672–681, 2015.

[30] Z. Ju, G. Ouyang, M. Wilamowska-Korsak, and H. Liu, "Surface emg based hand manipulation identification via nonlinear feature extraction and classification," *IEEE Sensors Journal*, vol. 13, no. 9, pp. 3302–3311, 2013.

[31] E. Noohi, M. Žefran, and J. L. Patton, "A model for human–human collaborative object manipulation and its application to human–robot interaction," *IEEE Transactions on Robotics*, vol. 32, no. 4, pp. 880–896, 2016.

[32] Y. Li, K. P. Tee, R. Yan, W. L. Chan, and Y. Wu, "A framework of human–robot coordination based on game theory and policy iteration," *IEEE Transactions on Robotics*, vol. 32, no. 6, pp. 1408–1418, 2016.

[33] D. Erickson, M. Weber, and I. Sharf, "Contact stiffness and damping estimation for robotic systems," *The International Journal of Robotics Research*, vol. 22, no. 1, pp. 41–57, 2003.

[34] L. Rozo, S. Calinon, D. G. Caldwell, P. Jimenez, and C. Torras, "Learning physical collaborative robot behaviors from human demonstrations," *IEEE Transactions on Robotics*, vol. 32, no. 3, pp. 513–527, 2016.

[35] L. Peternel, T. Petrič, E. Oztop, and J. Babič, "Teaching robots to cooperate with humans in dynamic manipulation tasks based on multi-modal human-in-the-loop approach," *Autonomous robots*, vol. 36, no. 1-2, pp. 123–136, 2014.

[36] Y. Li and S. S. Ge, "Impedance learning for robots interacting with unknown environments," *IEEE Transactions on Control Systems Technology*, vol. 22, no. 4, pp. 1422–1432, 2014.

[37] Z. Li, B. Huang, A. Ajoudani, C. Yang, C.-Y. Su, and A. Bicchi, "Asymmetric bimanual control of dual-arm exoskeletons for human-cooperative manipulations," *IEEE Transactions on Robotics*, vol. 34, no. 1, pp. 264–271, 2018.

[38] T. Tsuji, P. G. Morasso, K. Goto, and K. Ito, "Human hand impedance characteristics during maintained posture," *Biological cybernetics*, vol. 72, no. 6, pp. 475–485, 1995.

[39] M. S. Erden and A. Billard, "End-point impedance measurements across dominant and nondominant hands and robotic assistance with directional damping," *IEEE Transactions on Cybernetics*, vol. 45, no. 6, pp. 1146–1157, 2015.

[40] W. He, S. S. Ge, and D. Huang, "Modeling and vibration control for a nonlinear moving string with output constraint," *IEEE/ASME Transactions on Mechatronics*, vol. 20, no. 4, pp. 1886–1897, 2015.

[41] M. Chen and G. Tao, "Adaptive fault-tolerant control of uncertain nonlinear large-scale systems with unknown dead zone," *IEEE Transactions on Cybernetics*, vol. 46, no. 8, pp. 1851–1862, 2016.

[42] P. Huang, F. Zhang, J. Cai, D. Wang, Z. Meng, and J. Guo, "Dexterous tethered space robot: Design, measurement, control, and experiment," *IEEE Transactions on Aerospace and Electronic Systems*, vol. 53, no. 3, pp. 1452–1468, 2017.

[43] D. Wang, H. He, and D. Liu, "Adaptive critic nonlinear robust control: a survey," *IEEE Transactions on Cybernetics*, vol. 47, no. 10, pp. 3429–3451, 2017.

[44] H. Wang, C. Wang, W. Chen, X. Liang, and Y. Liu, "Three-dimensional dynamics for cable-driven soft manipulator," *IEEE/ASME Transactions on Mechatronics*, vol. 22, no. 1, pp. 18–28, 2017.

[45] Y. Song, X. Huang, and C. Wen, "Tracking control for a class of unknown nonsquare MIMO nonaffine systems: A deep-rooted information based robust adaptive approach," *IEEE Transactions on Automatic Control*, vol. 61, no. 10, pp. 3227–3233, 2016.

[46] Y. Kang, D.-H. Zhai, G.-P. Liu, Y.-B. Zhao, and P. Zhao, "Stability analysis of a class of hybrid stochastic retarded systems under asynchronous switching," *IEEE Transactions on Automatic Control*, vol. 59, no. 6, pp. 1511–1523, 2014.

[47] G. Xie, L. Sun, T. Wen, X. Hei, and F. Qian, "Adaptive transition probability matrix-based parallel IMM algorithm," *IEEE Transactions on Systems, Man, and Cybernetics: Systems, DOI: 10.1109/TSMC.2019.2922305*, 2019.

[48] H. Yang and J. Liu, "An adaptive RBF neural network control method for a class of nonlinear systems," *IEEE/CAA Journal of Automatica Sinica*, vol. 5, no. 2, pp. 457–462, 2018.

[49] P. Huang, D. Wang, Z. Meng, F. Zhang, and Z. Liu, "Impact dynamic modeling and adaptive target capturing control for tethered space robots with uncertainties," *IEEE/ASME Transactions on Mechatronics*, vol. 21, no. 5, pp. 2260–2271, 2016.

[50] S.-L. Dai, M. Wang, and C. Wang, "Neural learning control of marine surface vessels with guaranteed transient tracking performance," *IEEE Transactions on Industrial Electronics*, vol. 63, no. 3, pp. 1717–1727, 2016.

[51] S.-L. Dai, C. Wang, and M. Wang, "Dynamic learning from adaptive neural network control of a class of nonaffine nonlinear systems," *IEEE Transactions on Neural Networks and Learning Systems*, vol. 25, no. 1, pp. 111–123, 2014.

[52] B. Xu, D. Wang, Y. Zhang, and Z. Shi, "Dob-based neural control of flexible hypersonic flight vehicle considering wind effects," *IEEE Transactions on Industrial Electronics*, vol. 64, no. 11, pp. 8676–8685, 2017.

[53] D. Wang, D. Liu, H. Li, B. Luo, and H. Ma, "An approximate optimal control approach for robust stabilization of a class of discrete-time nonlinear systems with uncertainties," *IEEE Transactions on Systems, Man, and Cybernetics: Systems*, vol. 46, no. 5, pp. 713–717, 2016.

[54] H. Wang, R. Zhang, W. Chen, X. Liang, and R. Pfeifer, "Shape detection algorithm for soft manipulator based on fiber bragg gratings," *IEEE/ASME Transactions on Mechatronics*, vol. 21, no. 6, pp. 2977–2982, 2016.

[55] W. He, S. S. Ge, Y. Li, E. Chew, and Y. S. Ng, "Neural network control of a rehabilitation robot by state and output feedback," *Journal of Intelligent & Robotic Systems*, vol. 80, no. 1, pp. 15–31, 2015.

[56] M. Bridges, D. M. Dawson, and C. Abdallah, "Control of rigid-link, flexible-joint robots: a survey of backstepping approaches," *Journal of Field Robotics*, vol. 12, no. 3, pp. 199–216, 1995.

[57] S. Zhang, Y. Dong, Y. Ouyang, Z. Yin, and K. Peng, "Adaptive neural control for robotic manipulators with output constraints and uncertainties," *IEEE Transactions on Neural Networks and Learning Systems*, vol. 29, no. 11, pp. 5554–5564, 2018.

[58] Y.-J. Liu, S. Tong, C. P. Chen, and D.-J. Li, "Neural controller design-based adaptive control for nonlinear MIMO systems with unknown

hysteresis inputs," *IEEE Transactions on Cybernetics*, vol. 46, no. 1, pp. 9–19, 2016.
[59] Z. Zhang, S. Xu, and B. Zhang, "Exact tracking control of nonlinear systems with time delays and dead-zone input," *Automatica*, vol. 52, pp. 272–276, 2015.
[60] W. He, X. He, and C. Sun, "Vibration control of an industrial moving strip in the presence of input deadzone," *IEEE Transactions on Industrial Electronics*, vol. 64, no. 6, pp. 4680–4689, 2017.
[61] Y. Jian, D. Huang, J. Liu, and D. Min, "High-precision tracking of piezoelectric actuator using iterative learning control and direct inverse compensation of hysteresis," *IEEE Transactions on Industrial Electronics*, vol. 66, no. 1, pp. 368–377, 2019.
[62] W. He, T. Meng, X. He, and S. S. Ge, "Unified iterative learning control for flexible structures with input constraints," *Automatica*, vol. 96, pp. 326–336, 2018.
[63] C. Yang, X. Wang, Z. Li, Y. Li, and C.-Y. Su, "Teleoperation control based on combination of wave variable and neural networks," *IEEE Transactions on Systems, Man, and Cybernetics: Systems*, vol. 47, no. 8, pp. 2125–2136, 2017.
[64] C. Yang, Y. Jiang, Z. Li, W. He, and C.-Y. Su, "Neural control of bimanual robots with guaranteed global stability and motion precision," *IEEE Transactions on Industrial Informatics*, vol. 13, no. 3, pp. 1162–1171, 2017.
[65] Z. Li, J. Li, and Y. Kang, "Adaptive robust coordinated control of multiple mobile manipulators interacting with rigid environments," *Automatica*, vol. 46, no. 12, pp. 2028–2034, 2010.
[66] C. P. Chen, G.-X. Wen, Y.-J. Liu, and Z. Liu, "Observer-based adaptive backstepping consensus tracking control for high-order nonlinear semi-strict-feedback multiagent systems," *IEEE Transactions on Cybernetics*, vol. 46, no. 7, pp. 1591–1601, 2016.
[67] Z. Li, Z. Chen, J. Fu, and C. Sun, "Direct adaptive controller for uncertain MIMO dynamic systems with time-varying delay and dead-zone inputs," *Automatica*, vol. 63, pp. 287–291, 2016.
[68] B. Xu and F. Sun, "Composite intelligent learning control of strict-feedback systems with disturbance," *IEEE Transactions on Cybernetics*, vol. 48, no. 2, pp. 730–741, 2018.
[69] B. Gao, P. Lu, W. L. Woo, G. Y. Tian, Y. Zhu, and M. Johnston, "Variational bayesian sub-group adaptive sparse component extraction for diagnostic imaging system," *IEEE Transactions on Industrial Electronics*, 2018.
[70] X. Xie, D. Yang, and H. Ma, "Observer design of discrete-time T–S fuzzy systems via multi-instant homogenous matrix polynomials," *IEEE Transactions on Fuzzy Systems*, vol. 22, no. 6, pp. 1714–1719, 2014.
[71] Y. Zhang, J. Sun, H. Liang, and H. Li, "Event-triggered adaptive tracking control for multiagent systems with unknown disturbances," *IEEE Transactions on Cybernetics, DOI: 10.1109/TCYB.2018.2869084*, 2018.
[72] R. Martinez-Cantin, N. de Freitas, E. Brochu, J. Castellanos, and A. Doucet, "A bayesian exploration-exploitation approach for optimal online sensing and planning with a visually guided mobile robot," *Autonomous Robots*, vol. 27, no. 2, pp. 93–103, 2009.
[73] M. Mirkhani, R. Forsati, A. M. Shahri, and A. Moayedikia, "A novel efficient algorithm for mobile robot localization," *Robotics and Autonomous Systems*, vol. 61, no. 9, pp. 920–931, 2013.
[74] A. Petrovskaya, O. Khatib, S. Thrun, and A. Y. Ng, "Bayesian estimation for autonomous object manipulation based on tactile sensors," in *Proceedings 2006 IEEE International Conference on Robotics and Automation*, pp. 707–714, IEEE, 2006.
[75] T. Tsumugiwa, R. Yokogawa, and K. Hara, "Variable impedance control based on estimation of human arm stiffness for human-robot cooperative calligraphic task," in *Proceedings 2002 IEEE International Conference on Robotics and Automation*, vol. 1, pp. 644–650, IEEE, 2002.
[76] C. Yang, G. Ganesh, S. Haddadin, S. Parusel, A. Albu-Schaeffer, and E. Burdet, "Human-like adaptation of force and impedance in stable and unstable interactions," *IEEE Transactions on Robotics*, vol. 27, no. 5, pp. 918–930, 2011.
[77] Y. Li, S. S. Ge, Q. Zhang, and T. H. Lee, "Neural networks impedance control of robots interacting with environments," *IET Control Theory & Applications*, vol. 7, no. 11, pp. 1509–1519, 2013.
[78] S. S. Ge and C. Wang, "Adaptive nn control of uncertain nonlinear pure-feedback systems," *Automatica*, vol. 38, no. 4, pp. 671–682, 2002.

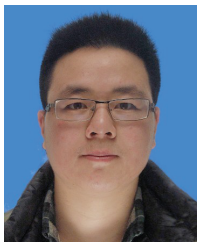

Xinbo Yu (S'16) received the B.E. degree in control technology and instrument from the School of Automation and Electrical Engineering, University of Science and Technology Beijing, Beijing, China, in 2013, where he is currently pursuing the Ph.D. degree in control theory and control engineering. His current research interests include adaptive neural networks control, robotics and human-robot interaction.

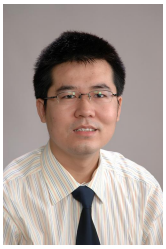

Wei He (S'09-M'12-SM'16) received his B.Eng. in automation and his M.Eng. degrees in control science and engineering from College of Automation Science and Engineering, South China University of Technology (SCUT), China, in 2006 and 2008, respectively, and his Ph.D. degree in control science and engineering from from Department of Electrical & Computer Engineering, the National University of Singapore (NUS), Singapore, in 2011.

He is currently working as a full professor in School of Automation and Electrical Engineering, University of Science and Technology Beijing, Beijing, China. He has co-authored 2 books published in Springer and published over 100 international journal and conference papers. He was awarded a Newton Advanced Fellowship from the Royal Society, UK in 2017. He was a recipient of the IEEE SMC Society Andrew P. Sage Best Transactions Paper Award in 2017. He is serving the Chair of IEEE SMC Society Beijing Capital Region Chapter. He is serving as an Associate Editor of *IEEE Transactions on Neural Networks and Learning Systems*, *IEEE Transactions on Control Systems Technology*, *IEEE Transactions on Systems, Man, and Cybernetics: Systems*, *IEEE/CAA Journal of Automatica Sinica*, *Neurocomputing*, and an Editor of *Journal of Intelligent & Robotic Systems*. His current research interests include robotics, distributed parameter systems and intelligent control systems.

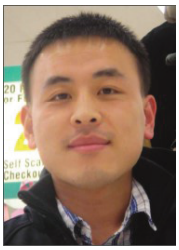

Yanan Li (S'10-M'14) is a Lecturer in Control Engineering with the Department of Engineering and Design, University of Sussex, UK. He received the B.Eng. and M.Eng. degrees from the Harbin Institute of Technology, China, in 2006 and 2008, respectively, and the PhD degree from the National University of Singapore, in 2013.

From 2015 to 2017, he has been a Research Associate with the Department of Bioengineering, Imperial College London, UK. From 2013 to 2015, he has been a Research Scientist with the Institute for Infocomm Research (I2R), Agency for Science, Technology and Research (A*STAR), Singapore. Dr Li has active research in human-robot interaction and robot control and their applications in semi-autonomous industrial robots, tele-operation robots and rehabilitation robots. He has served as Technical Committee on Bio-mechatronics and Bio-robotics Systems and Technical Committee on Autonomous Bionic Robotic Aircraft, IEEE Systems, Man, and Cybernetics Society, and International Program Committee Member and Session Chair for several conferences in robotics and control. He has led and participated in several research projects funded by Xiamen Municipal Government, EU, Singapore SERC, MDA, etc.

Chengqian Xue received the B.E. degree in automation (Excellence Program) from the School of Advanced Engineering, University of Science and Technology Beijing, Beijing, China, in 2018, he is currently pursuing the M.E. degree in control science and engineering from the School of Automation and Electrical Engineering, University of Science and Technology Beijing, Beijing, China. His current research interests include adaptive neural networks control, robotics and human-robot interaction.

Jianqiang Li received the B.S. and Ph.D. degrees from the South China University of Technology, Guangzhou, China, in 2003 and 2008, respectively. He is a Professor with the College of Computer and Software Engineering, Shenzhen University, Shenzhen, China. He led three projects of the National Natural Science Foundation and a project of the Natural Science Foundation of Guangdong Province, Shenzhen. His current research interests include robotic, hybrid systems, Internet of Thing, and embedded systems.

Jianxiao Zou (M'15) received his B.S., M.S. and Ph.D. degrees in Control Science and Engineering from the University of Electronic Science and Technology of China (UESTC), Chengdu, China, in 2000, 2003 and 2009, respectively. He is presently working as a Professor at UESTC, and has been serving as the Vice Dean of the School of Automation Engineering since 2011. He was a Visiting Scholar at the University of California, Berkeley, CA, USA, in 2010; and a Senior Visiting Professor at Rutgers, the State University of New Jersey, New Brunswick, NJ, USA, in 2014. His current research interests include control theory and control engineering, renewable energy control technologies, intelligent information processing and control.

Chenguang Yang (M'10-SM'16) is a Professor of Robotics. He received the Ph.D. degree in control engineering from the National University of Singapore, Singapore, in 2010 and performed postdoctoral research in human robotics at Imperial College London, London, UK from 2009 to 2010. He has been awarded EU Marie Curie International Incoming Fellowship, UK EPSRC UKRI Innovation Fellowship, and the Best Paper Award of the IEEE Transactions on Robotics as well as over ten conference Best Paper Awards. His research interest lies in human robot interaction and intelligent system design.